International Journal of Nanomedicine

Dovepress

open access to scientific and medical research

Open Access Full Text Article

ORIGINAL RESEARCH

Gold Nanostars: A Novel Platform for Developing ^{211}At-Labeled Agents for Targeted Alpha-Particle Therapy

Yang Liu[1]
Zhengyuan Zhou[2]
Yutian Feng[2]
Xiao-Guang Zhao[2]
Ganesan Vaidyanathan[2]
Michael R Zalutsky[1,2]
Tuan Vo-Dinh[1,3,4]

[1]Department of Biomedical Engineering, Duke University, Durham, NC, 27708, USA; [2]Department of Radiology, Duke University Medical Center, Durham, NC, 27710, USA; [3]Department of Chemistry, Duke University, Durham, NC, 27708, USA; [4]Fitzpatrick Institute for Photonics, Duke University, Durham, NC, 27708, USA

Aim: To develop an innovative ^{211}At nanoplatform with high radiolabeling efficiency and low in vivo deastatination for future targeted alpha-particle therapy (TAT) to treat cancer.

Methods: Star-shaped gold nanoparticles, gold nanostars (GNS), were used as the platform for ^{211}At radiolabeling. Radiolabeling efficiency under different reaction conditions was tested. Uptake in the thyroid and stomach after systemic administration was used to evaluate the in vivo stability of ^{211}At-labeled GNS. A subcutaneous U87MG human glioma xenograft murine model was used to preliminarily evaluate the therapeutic efficacy of ^{211}At-labeled GNS after intratumoral administration.

Results: The efficiency of labeling GNS with ^{211}At was almost 100% using a simple and rapid synthesis process that was completed in only 1 min. In vitro stability test in serum showed that more than 99% of the ^{211}At activity remained on the GNS after 24 h incubation at 37°C. In vivo biodistribution results showed low uptake in the thyroid (0.44–0.64%ID) and stomach (0.21–0.49%ID) between 0.5 and 21 h after intravenous injection, thus indicating excellent in vivo stability of ^{211}At-labeled GNS. The preliminary therapeutic efficacy study demonstrated that ^{211}At labeled GNS substantially reduced tumor growth ($P < 0.001$; two-way ANOVA) after intratumoral administration.

Conclusion: The new ^{211}At radiolabeling strategy based on GNS has the advantages of a simple process, high labeling efficiency, and minimal in vivo dissociation, making it an attractive potential platform for developing TAT agents that warrants further evaluation in future preclinical studies directed to evaluating prospects for clinical translation.

Keywords: astatine-211, ^{211}At, gold nanostars, GNS, cancer therapy, targeted alpha-particle therapy, TAT

Introduction

Targeted alpha-particle therapy (TAT) is an emerging method for cancer treatment that has the advantages of high linear energy transfer (>50 keV/μm), irreparable double-strand DNA breaks, and independence of dose rate, cell cycle, and cellular oxygenation.[1,2] As a result, TAT is conceptually superior to standard-of-care external beam radiation therapy using X-rays or γ-rays particularly for treating hypoxic tumors. Furthermore, since alpha-particles have a range of only a few cell diameters, TAT is an attractive approach for treating disseminated cancers.[3] Among the different available alpha-particle emitting radionuclides, astatine-211 (^{211}At) has the unique advantages of an optimal half-life (7.2 h) and absence of long-lived alpha-particle emitting daughter radionuclides, thus preventing off-target radiation toxicity from the

Correspondence: Michael R Zalutsky
Department of Radiology, Duke University Medical Center, 311 Research Drive, 161H Bryan Research Building, Durham, NC, 27710, USA
Email michael.zalutsky@duke.edu

Tuan Vo-Dinh
Department of Biomedical Engineering, Duke University, 1427 CIEMAS, Box 90281, Durham, NC, 27708, USA
Tel +1 919 660-8520
Email tuan.vodinh@duke.edu

Received: 2 July 2021
Accepted: 28 August 2021
Published: 28 October 2021

redistribution of daughter radionuclides.[2,4] Our group performed the first clinical trial for the treatment of glioblastoma (GBM) with ^{211}At-labeled antibodies.[5] However, traditional ^{211}At radiolabeling methods including the one used in this clinical study generate a chemical bond between ^{211}At and an aromatic carbon that have the following limitations: (1) the complicated radiochemistry process makes it difficult for clinical applications; (2) low conjugation efficiency results could lead to suboptimal cancer treatment: only 1 in 400 to 1000 antibody molecules can be labeled with an ^{211}At; (3) the ^{211}At from the labeled molecule can dissociate from the prosthetic moiety due to intrinsic low C-At bond strength and in vivo metabolic degradation.[6,7] Innovative radiolabeling methods involving a simple process, high yield, and loading capacity are urgently needed for both preclinical studies and clinical translation of TAT agents labeled with ^{211}At.

Our group has developed a novel method to synthesize star-shaped gold nanoparticles, gold nanostars (GNS), for biomedical applications without the need for toxic surfactants.[8] The multibranched GNS morphology offered a high surface area for ^{211}At labeling, which helped achieve a very effective delivery platform. Furthermore, the size of GNS can be tailored to optimize the preferential accumulation in tumors by the enhanced permeability and retention effect. In prior studies, we have demonstrated that the developed GNS can accumulate selectively in brain cancer mediated by the enhanced permeability and retention effect.[9] The enhanced permeability and retention effect was reported to be due to the tumor leaky vasculature, and this effect was found in most solid tumors.[10,11] Brain cancer was selected as the intended target disease for this study because it is one of the most aggressive cancers. Specifically, GBM, with more than 10,000 newly diagnosed patients in the United States each year, is the most common primary brain cancer.[12,13] Despite the highest first-year cost (> $120,000) for a cancer type, the prognosis for GBM patients is dismal. The median survival for GBM patients is only 15 months after aggressive treatments, including surgery, chemotherapy, and radiation therapy.[14–16] Less than 5% of the patients survive for more than 3 years.[17] Despite decades of effort, GBM is still a deadly disease with essentially 100% mortality.[18,19] Thus, there is a critical and urgent need to develop new approaches for effective brain cancer treatment.

As a first step towards developing a GNS-based ^{211}At-labeled TAT agent for GBM treatment, we have performed experiments described herein evaluating the potential utility of ^{211}At-labeled GNS for this purpose. Only a few studies have been reported directed at developing nanoparticle-driven carrier systems for use with ^{211}At. Ultrashort, single-walled carbon nanotubes (US-tubes) labeled with ^{211}At via noncovalent van der Waals binding have been evaluated in an ex vivo study.[20] However, the radiolabeling efficiency was low, and the in vivo stability of ^{211}At-labeled US-tubes was not studied. Although in vitro cell experiments have been performed with ^{211}At-labeled gold nanospheres, no in vivo investigations of gold nanoparticles have been described to date.[21,22]

In the current study, we evaluated GNS as a novel platform technology for ^{211}At radiolabeling and for the first time, investigated in vivo stability and biodistribution in normal mice, and therapeutic efficacy of the ^{211}At-GNS in a murine subcutaneous GBM model. Our experimental results showed that ^{211}At labeling of GNS can be achieved by a simple process in a short time with a high labeling efficiency and in vivo stability. In addition, the ^{211}At-labeled GNS demonstrated a substantial therapeutic efficacy by inhibiting tumor growth after intratumoral administration. To the best of our knowledge, this is the first in vivo study investigating gold nanoparticles as an ^{211}At delivery platform for future TAT applications.

Materials and Methods

GNS Synthesis and Characterization

All chemicals were purchased from Sigma-Aldrich unless mentioned otherwise. GNS were synthesized following our developed toxic surfactant-free and seed-mediated method reported in previous studies.[23,24] 12-nm spherical gold nanoparticles synthesized using the trisodium citrate reduction method were used as seeds. For GNS synthesis, 1 mL of 3 mM $AgNO_3$ in deionized (DI) water and 1 mL of 50 mM ascorbic acid in DI water were rapidly added to a mixture of 100 mL of DI water with 0.25 mM $HAuCl_4$, 1 mM HCl, and 1 mL of the 12-nm gold nanosphere seeds under vigorous stirring. After a 10-min reaction, 1 mL of 1 mM mPEG-SH (MW 6,000) in DI water was added and the mixture was incubated for 1 h at room temperature. The resultant GNS were purified and concentrated by centrifugation at 6000 g for 30 min. Transmission electron microscopy (TEM) of GNS was performed using a Tecnai G^2 Twin transmission electron microscope (FEI, Hillsboro, OR) with a 160 kV acceleration voltage. The Vis-NIR spectrum was obtained by using a UV-Vis-NIR spectrometer (UV-3600, Shimadzu, Japan). The hydrodynamic

diameter and nanoparticle concentration of the PEGylated GNS were measured with Nanoparticle Tracking Analysis method (Nanosight 500, Malvern, UK).

Radiolabeling and in vitro Stability

Astatine-211 was produced at the Duke University Medical Center cyclotron facility by bombarding a natural bismuth target with a 28.0-MeV alpha-particle beam and subsequently isolated by a dry distillation method.[25] For the radiolabeling experiments, 100 μg GNS in DI water were mixed with 7.4 MBq ^{211}At (460 fmol) in different media [DI water, 0.1 M NaOH in DI water, 50 mM ascorbic acid (AA) in DI water, or 0.2 mg/mL N-chlorosuccinimide (NCS) in DI water], and the reaction was allowed to proceed at room temperature for 1, 5 and 30 min. We also evaluated the effect of the GNS amount – ranging from 100 μg (540 fmol) down to 0.01 μg (54 amol) – on radiolabeling efficiency using a 5-min reaction time. The reaction volume was 100 μL, and centrifugation (6,000 g, 10 min) was used to separate free, unreacted ^{211}At remaining in solution and ^{211}At-labeled GNS. The ^{211}At-labeled GNS pellet was resuspended in 100 μL of DI water, and then the radioactivity levels were measured using a dose calibrator. The stability of ^{211}At-labeled GNS was evaluated by incubating it in phosphate-buffered saline (PBS), pH 7.4, and in murine serum at 37°C up to 24 h. The murine serum was isolated by centrifugating the murine whole blood at 3000 g for 10 min. The supernatant (serum) was collected for the in vitro stability measurements. The concentration of the ^{211}At-GNS agent in both the murine serum and PBS was 200 μg/mL (Au) with 7.4 MBq ^{211}At per mL. The same centrifugation protocol (6,000 g, 10 min) was used to separate dissociated ^{211}At in the solution and the ^{211}At-labeled GNS.

In vivo Biodistribution

Freshly prepared PEGylated GNS were labeled with ^{211}At by incubation at room temperature for 5 min in 50 mM ascorbic acid in DI water. Radiolabeled GNS were purified by centrifugation/washing 3 times and resuspended in PBS without ascorbic acid. For the biodistribution experiment, 20 nude mice were randomly divided into 4 groups, and each mouse was intravenously injected with ^{211}At-labeled GNS (0.185 MBq radioactivity and 100 μg gold mass) in 100 μL PBS without ascorbic acid. Mice were euthanized, and organs of interest (liver, spleen, lung, heart, kidney, bladder, stomach, small intestine, large intestine, thyroid, muscle, blood, urine, bone, skin, brain, and tail) were harvested at 0.5, 2, 14, and 21 h after intravenous injection of the radiolabeled GNS. Tissues were weighed and counted along with injection standards for ^{211}At activity using an automated gamma counter (LKB 1282, Wallac, Finland). The measurement geometry of the gamma counter was taken into account by placing samples at the same location as that for the standard. From these counts, the percent injected dose per gram tissue (%ID/g) and percent injected dose per organ (%ID/organ) were calculated using an in-house computer program.

Therapeutic Efficacy Experiment

Human glioma U87MG cells were obtained from Duke Cell Culture Facility and cultured in MEM cell growth medium with 10% fetal bovine serum (Hyclone, MA, USA), 100 units/mL penicillin, and 100 μg/mL streptomycin at 37°C in a 5% CO_2 incubator. The use of the U87MG cell line was approved by the ethics committee, and this cell line was authenticated by the short tandem repeat profiling. All animal studies were performed under protocols that had been approved by the Duke University Institutional Animal Care and Use Committee. The guidelines from National Institutes of Health and Duke University Institutional Animal Care and Use Committee were followed. For subcutaneous xenograft generation, 3×10^6 U87MG human glioma cells in the cell growth medium were subcutaneously injected into each mouse in the flank region. The tumor size was calculated as 0.5×length×width×width. After 18 days, the tumor size reached ~100 mm^3 and the intratumoral therapy study was initiated. Groups of 10 mice received either 30 μL of ^{211}At-labeled GNS (1.11 MBq) in PBS or just PBS by intratumoral injection using a syringe pump at a rate of 30 μL/min. The tumor sizes were measured every 3 or 4 days until the end of the study.

Results

The synthesized GNS exhibited a star-like shape and had a maximum absorption at 765 nm (Figure 1). We performed ^{211}At radiolabeling experiments using PEGylated GNS with a hydrodynamic diameter of 50 nm using different reaction conditions and the results are shown in Figure 2. First, we compared the radiolabeling efficiency in four different reaction media. The calculated ^{211}At labeling efficiency was 94.7 ± 0.1% in DI water, 97.4 ± 0.2% in DI water with 0.1 M NaOH, 99.8 ± 0.1% in DI water with 50 mM ascorbic acid, and 42.6 ± 0.3% in DI

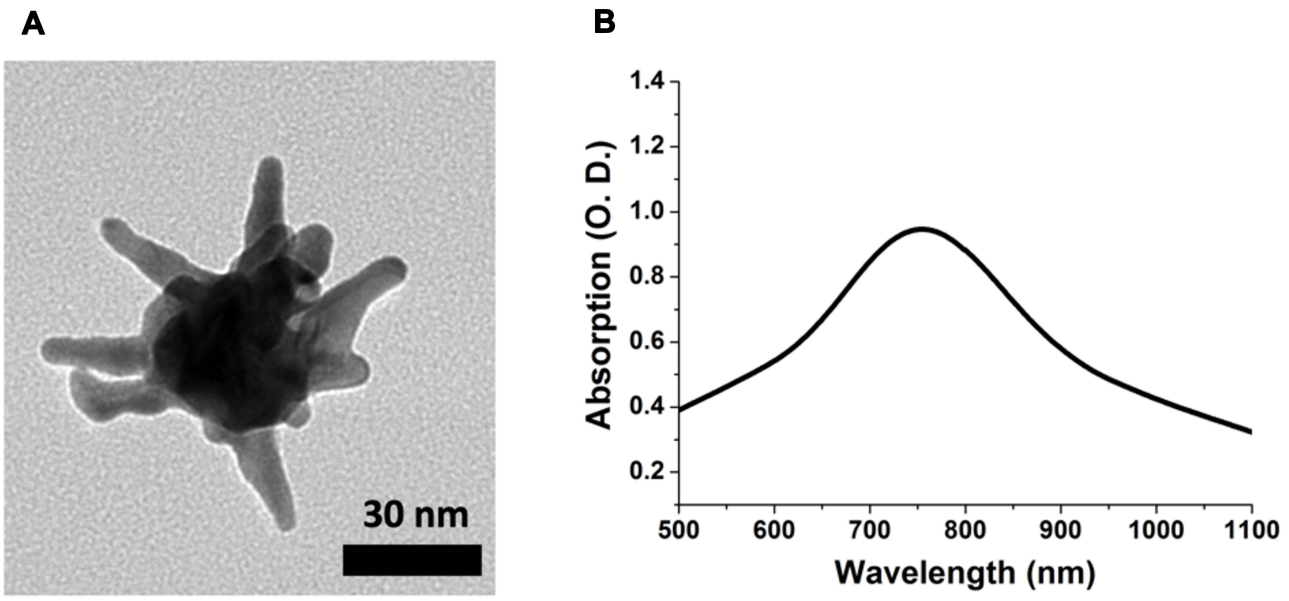

Figure 1 TEM image (**A**) and Vis-NIR absorption spectrum (**B**) of the synthesized GNS used in this study.

water with 0.2 mg/mL NCS. The radiolabeling efficiency for the reaction medium with a reducing agent, ascorbic acid, was the highest (99.8%), and almost all the ^{211}At could be attached to GNS after only a 5-min incubation at room temperature. Conversely, the NCS oxidizing agent dramatically decreased the radiolabeling efficiency to 42.6 ± 0.3%. Second, we evaluated the effect of incubation time on radiolabeling efficiency in reaction media consisting of DI water or DI water with 50 mM ascorbic acid. The radiolabeling efficiency in DI water increased from 93.4 ± 0.2% (1 min), to 94.7 ± 0.1% (5 min), and 97.4 ± 0.2% (30 min). The radiolabeling efficiency in DI water with 50 mM ascorbic acid was essentially quantitative by 1 min and remained constant over 30 min. Third, we compared how the nanoparticle-to-^{211}At ratio affected the radiolabeling using DI water with 50 mM ascorbic acid as the reaction medium. The radiolabeling efficiency decreased as the ^{211}At:GNS ratio increased: from 99.8 ± 0.1% (540 fmol GNS, ^{211}At:GNS = 0.85), 99.1 ± 0.1% (54 fmol GNS, ^{211}At:GNS = 8.5), 98.3 ± 0.1% (5.4 fmol GNS, ^{211}At:GNS = 85), 94.1 ± 0.2% (540 amol GNS, ^{211}At:GNS = 850), and 67.4 ± 0.2% (54 amol GNS, ^{211}At:GNS = 8,500). The in vitro stability tests at 37°C indicated that 99.5 ± 0.3% and 99.6 ± 0.2% ^{211}At remained on GNS after 1 h incubation in PBS and serum, respectively. After 24 h incubation, the percentage of ^{211}At on GNS was 98.9 ± 0.2% for PBS and 99.1 ± 0.3% for serum at 37°C.

After evaluating the feasibility of labeling GNS with ^{211}At, we performed a comprehensive study to investigate the biodistribution of ^{211}At activity in normal mice after intravenous injection of ^{211}At-labeled GNS. As shown in Figure 3, at 30 min, blood was found to have the highest concentration of ^{211}At activity (44.4 ± 4.5%ID/g) followed by spleen (22.6 ± 1.8%ID/g), lungs (16.9 ± 2.0%ID/g), liver (9.1 ± 2.2%ID/g) and kidneys (8.1 ± 1.1%ID/g). In total, nearly 60%ID was found in the blood pool and ~13% ID was found in the liver. Activity in the blood decreased with time between 0.5 and 21 h after intravenous injection – from 44.4 ± 4.5%ID/g at 0.5 h to 40.6 ± 3.2%ID/g, 22.9 ± 4.17%ID/g and 22.0 ± 4.7%ID/g remaining at 2, 14 and 21 h, respectively. Similar behavior was observed in the lungs. In contrast, the %ID/g in spleen increased with time, from 22.6 ± 1.9%ID/g at 0.5 h, to 37.5 ± 5.9%ID/g at 2 h, 35.3 ± 4.7%ID/g at 14 h, and 105.3 ± 15.8%ID/g at 21 h; a similar trend was observed in the liver. For radiohalogens like ^{211}At, uptake in the thyroid and the stomach can serve as an indicator of in vivo stability because of the proclivity of free halides for these tissues. The %ID in thyroid was low and did not change significantly between 0.5 and 21 h, with values of 0.61 ± 0.21%ID, 0.64 ± 0.28% ID, 0.44 ± 0.18%ID, and 0.61 ± 0.21%ID measured at 0.5, 2, 14 and 21 h, respectively. Likewise, the %ID in the stomach was low at all time points: 0.21 ± 0.06%ID at 0.5h, 0.28 ± 0.08%ID at 2h, 0.43 ± 0.14%ID at 14 h, and 0.49 ± 0.10%ID at 21 h. In summary, the biodistribution

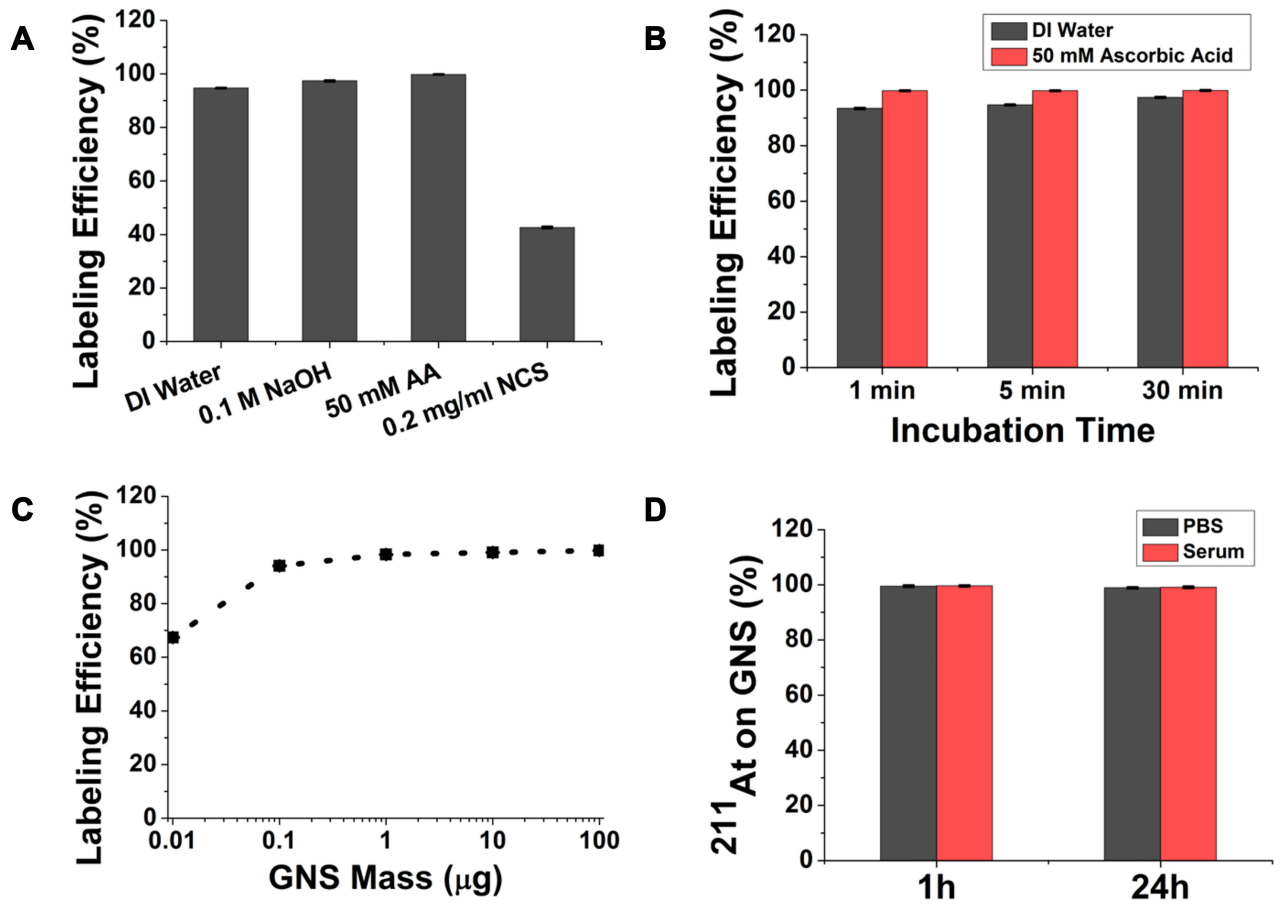

Figure 2 Evaluation of radiolabeling GNS with ^{211}At. (**A**). Radiolabeling efficiency evaluation in different reaction media: DI water, DI water with 0.1 M NaOH, DI water with 50 mM ascorbic acid, DI water with 0.2 mg/mL NCS after a 5 min incubation. (**B**) Radiolabeling efficiency as a function of incubation time when the reaction was performed using DI water or DI water with 50 mM ascorbic acid as the media. (**C**) Radiolabeling efficiency evaluation for GNS mass ranging from 0.01–100 μg for 5 min incubation in DI water with 50 mM ascorbic acid. (**D**) Percentage of ^{211}At remaining on GNS after incubation in PBS and murine serum at 37°C for 1 h and 24 h. All experiments performed in triplicate and error bar shows standard deviation.

results showed that ^{211}At-labeled GNS had a long circulation time in the blood and accumulated in the liver and spleen gradually, with a low degree of deastatination in vivo.

As an initial evaluation of the therapeutic potential of ^{211}At-labeled GNS, an experiment was performed in athymic mice with subcutaneous U87MG human glioma xenografts with the labeled drug given by the intratumoral route. As shown in Figure 4, the ^{211}At-labeled GNS substantially inhibited the tumor growth rate. The average tumor volume in the control group increased rapidly from 82 mm^3 on Day 1 to 177 mm^3, 409 mm^3, 798 mm^3, and 1456 mm^3 on Days 4, 7, 10, and 14, respectively. In contrast, the average tumor volume in the treatment group increased slowly, from 78 mm^3 on Day 1 to 95 mm^3, 112 mm^3, 152 mm^3, and 189 mm^3 on Days 4, 7, 10, and 14, respectively. The two-way ANOVA test indicated that the difference in tumor volumes between the ^{211}At-labeled GNS treated group and the control group with PBS injection was statistically significant ($P < 0.001$).

Discussion

The multibranched GNS morphology of GNS offered a high surface area for loading ^{211}At, which should provide a very effective delivery platform. Consistent with this expectation, our developed GNS had a very promising performance as a nanoplatform for ^{211}At delivery. First, the radiolabeling process is simple and can be completed as fast as 1 min with nearly quantitative labeling efficiency (99.8%). Moreover, the radiolabeling process can be performed without using the organic solvents or a high-performance liquid chromatography system for purification as is generally required for traditional radiolabeling methods based on At-C chemical bond formation. Second, the GNS loading capacity for ^{211}At is high and the radiolabeling efficiency remained at ~94% when an ^{211}At:GNS ratio

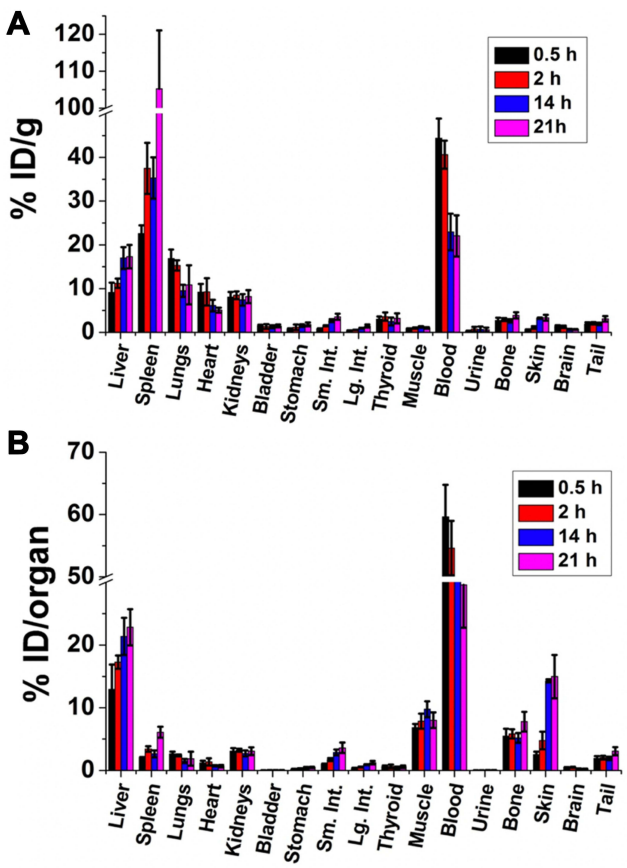

Figure 3 Biodistribution of ^{211}At activity after intravenous injection of ^{211}At-labeled GNS in normal mice. The results are shown as percent injected dose per gram tissue (%ID/g) (**A**), and as percent injected dose per organ (%ID/organ) (**B**). Error bar shows the standard deviation (n=5).

of 850 was used. The radiolabeling efficiency dropped to 67.4% when we further increased the ^{211}At:GNS ratio to 8,500, indicating that the maximum number of ^{211}At loaded per GNS was approximately 5,700. In contrast, traditional macromolecular radiolabeling methods based on At-C chemical bond formation generally have a low conjugation efficiency: only 1 in 400 to 1,000 antibody molecules can be labeled with an ^{211}At radionuclide.[2] Third, the ^{211}At-labeled GNS exhibited high stability and minimal in vivo dissociation. The thyroid and stomach are the two major organs that take up high amounts of free [^{211}At] astatide. We observed a low uptake of ^{211}At activity in the thyroid (0.44–0.61%ID) and the stomach (0.21–0.49%ID) between 0.5 h and 21 h after systemic administration of ^{211}At-labeled GNS, suggesting a low degree of in vivo dehalogenation had occurred.

The observed high in vivo stability of ^{211}At labeled GNS can be explained by the strong chemical bond formed between At and Au.[26] The calculated bond energy was reported to be 130 kJ/mol and the oxidation state for ^{211}At for binding to Au was considered to be −1.[26] Our radiolabeling results are consistent with this; in the presence of a reducing agent, ascorbic acid, ^{211}At labeling of GNS increased, while in the presence of an oxidizing agent, NCS, ^{211}At labeling of GNS decreased, indicating that the oxidization state of At on GNS is −1. We plan to perform mechanistic studies to better understand our

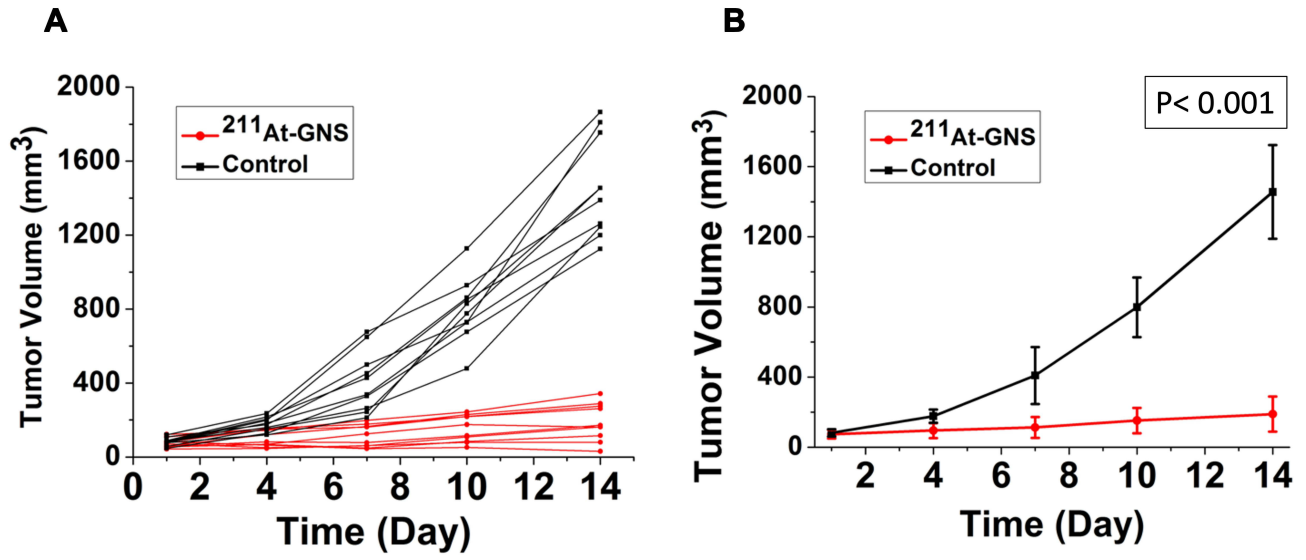

Figure 4 Therapeutic efficacy evaluation of ^{211}At TAT using GNS as a novel delivery platform. (**A**) tumor size change profile for each mouse in the ^{211}At-GNS treatment group (1.11 MBq) and blank control group with PBS injection. (**B**) Average tumor size change profile for mice in the ^{211}At-GNS treatment group (1.11 MBq) and blank control group with PBS injection. Error bar shows standard deviation (n = 10). P value was calculated using 2-way ANOVA (P< 0.001).

in vivo experimental data in the near future using approaches similar to those used by Teze et al.[6]

The in vivo stability of the ^{211}At-labeled TAT agent is critical because dissociated ^{211}At can result in off-targeted toxicity and decrease the radiation dose delivered to the tumor. To provide a frame of reference, we compared our in vivo stability results with those from previous studies in mice using clinically applied ^{211}At coupling reagents including N-succinimidyl 3-trimethylstannylbenzoate (m-MeATE) and isothiocyantophenethyl-ureido-closodecaborate(2-) (B10-NCS). Using a murine model, Zalutsky et al reported the stomach uptake for an ^{211}At-labeled antibody prepared using m-MeATE to be 2.94–4.07%ID/g between 0.5 and 24 h after IV injection with a thyroid uptake of 0.36–0.73%ID.[27] In a separate biodistribution study using the same m-MeATE reagent for labeling an antibody F(ab')$_2$ fragment with ^{211}At, Bäck et al reported that the stomach uptake was 4.4–12.3% ID/g during 0.5–21 h after IV injection,[28] which is significantly higher than that (0.71–1.79%ID/g) for our GNS delivery platform. Orozco et al utilized the B10-NCS coupling reagent to label an anti-CD45 antibody with ^{211}At and reported a stomach uptake of 1–2%ID/g between 1 h and 7 h, reaching ~5%ID/g at 24 h.[29]

We next compared our in vivo stability results with those for other ^{211}At TAT agents moving toward clinical trial including meta-[^{211}At]astatobenzylguanidine (^{211}At-MABG), and N-succinimidyl 3-((1,2-bis(tert-butoxycarbonyl)guanidino) methyl)-5-(trimethylstannyl)benzoate (Boc_2-iso-SGMTB). Ohshima et al reported that for ^{211}At-MABG, stomach uptake was 2.41–6.71%ID/g and thyroid uptake was 0.61–1.65%ID between 1 and 24 h after injection.[30] Choi et al utilized the Boc_2-iso-SGMTB linker to label a single-domain antibody fragment (sdAb) with ^{211}At and reported a stomach uptake of 0.5–1.7%ID/g and thyroid uptake of 0.15–0.35%ID over up to 24 h after injection.[7] In addition, there are some other ^{211}At-coupling reagents at earlier stages of development that provide data for comparison. For example, Dekempaner evaluated the N-[2-(maleimido)ethyl]-3-(trimethylstannyl) benzamide (MSB) coupling reagent in comparison to Boc_2-SGMTB, m-MeATE for labeling an sdAb with ^{211}At.[31] The reported stomach uptake for ^{211}At-labeled sdAb using MSB was more than 20%ID/g between 1 and 6 h after injection. Better in vivo stability was observed with sdAb labeled using m-MeATE, but stomach uptake was still more than 10%ID/g even at 1 h after injection. Consistent with the results of Choi et al,[7] ^{211}At-labeled sdAb prepared using Boc_2-SGMTB had the lowest stomach uptake among the three studied methods, with ~2%ID/g between 1 and 6 h after injection.

With regard to the in vivo stability of small organic molecule TAT agents labeled with ^{211}At, Ohshima reported that for [^{211}At]astatophenylalanine, stomach uptake was 0.6–2.99%ID/g during the first 6 h after injection.[32] Makvandi et al evaluated the in vivo stability of [^{211}At] MM4 (1-(4-astatophenyl)-8,9-dihydro-2,7,9atriazabenzo [cd]azulen-6(7H)-one) and stomach uptake was more than 10%ID/g within 2 h after injection.[33] Liu et al radiolabeled a small-molecule peptide with ^{211}At by using an N-succinimidyl 5-(tributylstannyl)-3-pyridinecarboxylate ester precursor and reported the stomach uptake to be 5.55%ID/g 3 h after intravenous injection.[34] However, in a subsequent therapy study using this molecule, gastric toxicity was observed at higher doses.[35] In summary, although different animal models were used, uptake of ^{211}At activity in the stomach and thyroid after injection of ^{211}At-labeled GNS is lower than that observed for most other ^{211}At-labeled TAT agents, including those that have either been investigated clinically or will soon enter clinical trials. This suggests that the GNS delivery platform has sufficient in vivo stability for future clinical translation.

It is worth noting that GNS have other properties that may provide advantages compared with more conventional gold nanoparticle configurations, particularly when combination therapeutic strategies are contemplated. GNS have tip-enhanced plasmonics with a dramatically increased electromagnetic field near the sharp tip, making them a superior nanoplatform for certain imaging and therapy approaches. For example, we have used GNS for in vivo surface-enhanced Raman spectroscopy for cancer detection in a sarcoma murine animal model.[36] In addition, we have used GNS for both in vitro and in vivo high-resolution imaging with two-photon photoluminescence. The GNS have an extremely high two-photon cross section, which is up to 4 orders of magnitude higher than that for gold nanospheres.[37] As a result, we can image a single GNS under two-photon photoluminescence imaging.[38] The GNS capability for sensitive optical imaging at the subcellular level makes it an attractive theranostic platform for image-guided therapy and to investigate the therapeutic efficacy of TAT with ^{211}At. We have also used GNS for photothermal therapy and our experimental results demonstrated that GNS are superior to gold nanoshells, which are under clinical trial to treat prostate cancer with photothermal therapy.[39] Therefore, GNS are an

attractive nanoplatform because they can be used for combining photothermal therapy and TAT with the aim of generating synergistically effective cancer treatments.

A preliminary therapeutic efficacy study on a human GBM flank tumor murine model demonstrated that TAT therapy with ^{211}At-labeled GNS can dramatically decrease tumor growth. With a high linear energy transfer, TAT therapy can generate irreparable DNA double-strand breaks with a therapeutic effect that is independent of tissue oxygen level, which is superior to traditional external beam radiation therapy. External beam radiation therapy is characterized as a low linear energy transfer, reparable DNA single-strand break generating radiation, with the requirement of oxygen to generate radical oxygen species for therapeutic effect. In previous studies, we radiolabeled these same GNS with ^{124}I and performed PET/CT imaging in mice with intracranial tumors and demonstrated that the GNS could accumulate selectively in brain tumors with tumor-to-normal ratios of up to 7.8:1.[9] In future studies, we plan to use a similar intracranial GBM murine animal model to evaluate the therapeutic efficacy of ^{211}At-labeled GNS in an orthotopic setting. Finally, the developed GNS nanoplatform can also be applied for TAT to treat other types of cancer and through the use of different targeting ligands.

Conclusion

In summary, we have developed a novel ^{211}At radiolabeling nanoplatform using biocompatible GNS and performed the first in vivo biodistribution and ^{211}At therapy study with gold nanoparticles. Our experimental results demonstrated that the developed nanoplatform has the advantages of a simple radiolabeling process, high radiolabeling efficiency and loading capacity, minimal in vivo dissociation, and potent therapeutic effect. As a result, our novel ^{211}At nanoplatform has a great potential to be applied for future preclinical studies and clinical translation aimed at benefiting cancer patients.

Acknowledgments

The authors would like to acknowledge the support from the US National Institutes of Health (R01EB028078) and the US Department of Defense (W81XWH1910684). The content of the information in this paper does not necessarily reflect the position or the policy of the government, and no official endorsement should be inferred.

Disclosure

The authors report no conflicts of interest in this work.

References

1. Poty S, Francesconi LC, McDevitt MR, et al. Alpha-emitters for radiotherapy: from basic radiochemistry to clinical studies-Part 1. *J Nucl Med*. 2018;59(6):878–884.
2. Zalutsky MR, Vaidyanathan G. Astatine-211-labeled radiotherapeutics: an emerging approach to targeted alpha-particle radiotherapy. *Curr Pharm Des*. 2000;6(14):1433–1455.
3. Poty S, Francesconi LC, McDevitt MR, et al. Alpha-emitters for radiotherapy: from basic radiochemistry to clinical studies-Part 2. *J Nucl Med*. 2018;59(7):1020–1027.
4. Meyer GJ. Astatine. *J Labelled Comp Radiopharm*. 2018;61(3):154–164.
5. Zalutsky MR, Reardon DA, Akabani G, et al. Clinical experience with alpha-particle emitting ^{211}At: treatment of recurrent brain tumor patients with ^{211}At-labeled chimeric antitenascin monoclonal antibody 81C6. *J Nucl Med*. 2008;49(1):30–38.
6. Teze D, Sergentu DC, Kalichuk V, et al. Targeted radionuclide therapy with astatine-211: oxidative dehalogenation of astatobenzoate conjugates. *Sci Rep*. 2017;7(1):2579.
7. Choi J, Vaidyanathan G, Koumarianou E, et al. Astatine-211 labeled anti-HER2 5F7 single domain antibody fragment conjugates: radiolabeling and preliminary evaluation. *Nucl Med Biol*. 2018;56:10–20.
8. Yuan H, Khoury CG, Hwang H, et al. Gold nanostars: surfactant-free synthesis, 3D modelling, and two-photon photoluminescence imaging. *Nanotechnology*. 2012;23(7):075102.
9. Liu Y, Carpenter AB, Pirozzi CJ, et al. Non-invasive sensitive brain tumor detection using dual-modality bioimaging nanoprobe. *Nanotechnology*. 2019;30(27):275101.
10. Maeda H. Tumor-selective delivery of macromolecular drugs via the EPR effect: background and future prospects. *Bioconj Chem*. 2010;21:797–802.
11. Maeda H. The enhanced permeability and retention (EPR) effect in tumor vasculature: the key role of tumor-selective macromolecular drug targeting. *Advan Enzyme Regul*. 2001;41:189–207.
12. Ostrom QT, Gittleman H, Fulop J, et al. CBTRUS statistical report: primary brain and central nervous system tumors diagnosed in the United States in 2008-2012. *Neuro Oncol*. 2015;17(Suppl4):iv1–iv62.
13. Davis ME. Glioblastoma: overview of disease and treatment. *Clin J Oncol Nurs*. 2016;20(5 Suppl):S2–8.
14. Mariotto AB, Yabroff KR, Shao Y, et al. Projections of the cost of cancer care in the United States: 2010-2020. *J Natl Cancer Inst*. 2011;103(2):117–128.
15. Stupp R, Mason WP, van den Bent MJ, et al. Radiotherapy plus concomitant and adjuvant temozolomide for glioblastoma. *N Engl J Med*. 2005;352(10):987–996.
16. Ningaraj NS, Salimath BP, Sankpal UT, et al. Targeted brain tumor treatment-current perspectives. *Drug Target Insights*. 2007;2:197–207.
17. Krex D, Klink B, Hartmann C, et al. Long-term survival with glioblastoma multiforme. *Brain*. 2007;130:2596–2606.
18. Omuro A, DeAngelis LM. Glioblastoma and other malignant gliomas: a clinical review. *JAMA*. 2013;310(17):1842–1850.
19. Ostrom QT, Bauchet L, Davis FG, et al. The epidemiology of glioma in adults: a "state of the science" review. *Neuro-Oncology*. 2014;16(7):896–913.
20. Hartman KB, Hamlin DK, Wilbur S, et al. ^{211}AtCl@US-Tube nanocapsules: a new concept in radiotherapeutic-agent design. *Small*. 2007;3(9):1496–1499.
21. Dziawer L, Koźmiński P, Męczyńska-Wielgosz S, et al. Gold nanoparticle bioconjugates labelled with ^{211}At for targeted alpha therapy. *RSC Adv*. 2017;7:41024–41032.
22. Dziawer L, Majkowska-Pilip A, Gaweł D, et al. Trastuzumab-modified gold nanoparticles labeled with ^{211}At as a prospective tool for local treatment of HER2-positive breast cancer. *Nanomaterials*. 2019;9:632.

23. Liu Y, Chongsathidkiet P, Crawford BM, et al. Plasmonic gold nanostar-mediated photothermal immunotherapy for brain tumor ablation and immunologic memory. *Immunotherapy*. 2019;11(15):1293–1302.
24. Liu Y, Maccarini P, Palmer GM, et al. Synergistic immuno photothermal nanotherapy (SYMPHONY) for the treatment of unresectable and metastatic cancers. *Sci Rep*. 2017;7(1):8606.
25. Feng Y, Zalutsky MR. Production, purification and availability of ^{211}At: near term steps toward global access. *Nucl Med Biol*. 2021;100:12–23.
26. Demidov Y, Zaitsevskii A. Adsorption of the astatine species on a gold surface: a relativistic density functional theory study. *Chem Phys Lett*. 2018;691:126–130.
27. Zalutsky M, Stabin MG, Larsen RH, et al. Tissue distribution and radiation dosimetry of astatine-211-labeled chimeric 81C6, an α -particle-emitting immunoconjugate. *Nucl Med Biol*. 1997;24:255–261.
28. Bäck T, Andersson H, Divgi CR, et al. ^{211}At radioimmunotherapy of subcutaneous human ovarian cancer xenografts: evaluation of relative biologic effectiveness of an α-Emitter in vivo. *J Nucl Med*. 2005;46 (12):2061–2067.
29. Orozco JJ, Bäck T, Kenoyer A, et al. Anti-CD45 radioimmunotherapy using ^{211}At with bone marrow transplantation prolongs survival in a disseminated murine leukemia model. *Blood*. 2013;121(18):3759–3767.
30. Ohshima Y, Sudo H, Watanabe S, et al. Antitumor effects of radionuclide treatment using α-emitting meta-^{211}At-astatobenzylguanidine in a PC12 pheochromocytoma model. *Eur J Nucl Med Mol Imaging*. 2018;45:999–1010.
31. Dekempeneer Y, Bäck T, Aneheim E, et al. Labeling of anti-HER2 nanobodies with astatine-211: optimization and the effect of different coupling reagents on their in vivo behavior. *Mol Pharm*. 2019; 16:3524–3533.
32. Ohshima Y, Suzuki H, Hanaoka H, et al. Preclinical evaluation of new α-radionuclide therapy targeting LAT1: 2-[^{211}At]astato-α-methyl -L-phenylalanine in tumor-bearing model. *Nucl Med Biol*. 2020;90–91:15–22.
33. Makvandi M, Lee H, Puentes LN, et al. Targeting PARP-1 with alpha-particles is potently cytotoxic to human neuroblastoma in preclinical models. *Mol Cancer Ther*. 2019;18:1195–1204.
34. Liu W, Ma H, Tang Y, et al. One-step labelling of a novel small-molecule peptide with astatine-211: preliminary evaluation in vitro and in vivo. *J Radioanal Nucl Chem*. 2018;316:451–456.
35. Liu W, Tang Y, Ma H, et al. Astatine-211 labelled a small molecule peptide: specific cell killing in vitro and targeted therapy in a nude-mouse model. *Radiochim Acta*. 2021;109(2):119–126.
36. Liu Y, Ashton JR, Moding EJ, et al. A plasmonic gold nanostar theranostic probe for in vivo tumor imaging and photothermal therapy. *Theranostics*. 2015;5(9):946–960.
37. Gao N, Chen Y, Li L, et al. Shape-dependent two-photon photoluminescence of single gold nanoparticles. *J Phys Chem C*. 2014;118 (25):13904–13911.
38. Liu Y, Huang W, Xiong C, et al. Biodistribution and sensitive tracking of immune cells with plasmonic gold nanostars. *Int J Nanomedicine*. 2019;14:3403–3411.
39. Rastinehad AR, Anastos H, Wajswol E, et al. Gold nanoshell-localized photothermal ablation of prostate tumors in a clinical pilot device study. *Proc Natl Acad Sci USA*. 2019;116:18590–18596.